Contents lists available at ScienceDirect

Journal of Physics and Chemistry of Solids

Cation mobility and structural changes on the water removal in zeolite-like zinc hexacyanometallates (II)

M. Avila [a], J. Rodríguez-Hernández [a,b], A.A. Lemus-Santana [a], E. Reguera [a,*]

[a] Center for Applied Science and Advanced Technology of IPN, México D.F., Mexico
[b] Institute of Materials Science and Technology, University of Havana, Havana, Cuba

ARTICLE INFO

ABSTRACT

The cation (A^+) mobility and structural changes on the water molecules removal in zeolite-like zinc hexacyanometallates series, $Zn_3A_2[Fe(CN)_6]_2 \cdot xH_2O$ with A=Na, K, Rb and Cs, were studied from X-ray diffraction data recorded for hydrated and anhydrous samples at room temperature and at 77 K. The crystal structure for the anhydrous phases were solved and refined and then compared with those corresponding to their hydrated form. On the water molecules removal the charge balancing cation (A^+) migrates to favor a stronger interaction with the N ends of the CN bridges where the framework negative charge is located. This cation–framework interaction model is supported by the recorded IR spectra for both hydrated and anhydrous samples. The new cation position induces distortion for both the cavity shape and their windows and also leads to cavity volume reduction. This is relevant for the properties of this family of solids as porous materials and their behavior in adsorption and separation processes, among them for hydrogen storage.

© 2011 Elsevier Ltd. All rights reserved.

1. Introduction

Zeolite-like zinc hexacyanometallates (II), $Zn_3A_2[M(CN)_6]_2 \cdot xH_2O$ with A=Na, K, Rb and Cs, and M=Fe, Ru and Os, in the following $Zn_3A_2M_2 \cdot xH_2O$, have received certain attention as prototype of porous solids for hydrogen storage [1–4]. The porous framework of these solids is formed by ellipsoidal cavities of ca. $12.5 \times 9 \times 8$ Å^3, which remain communicated by elliptical windows of about 5 Å [5–10]. The exchangeable metal (A^+) is found within these cavities, close to cavity windows. The metal (A^+) represents a charge center able to favor the H_2 stabilization within the cavity by electrostatic type interactions. The electrostatic interactions are related to the permanent quadrupole moment of the hydrogen molecule and to the polarization of its electron cloud by a charge center [4]. A molecule with quadrupole moment interacts with an electric field gradient. The strength of the polarization interaction depends on the local electric field, and from this fact porous materials with exchangeable metals are particularly attractive for H_2 storage. Such a possibility has been considered for H_2 storage in zeolites [11,12]. However in zeolites the ion polarizing power is partially shielded by the framework oxygen atoms electron cloud [12], an effect less pronounced for zeolite-like zinc hexacyanometallates [2]. From the recorded H_2 adsorption isotherms in $Zn_3A_2[M(CN)_6]_2$ evidence on the cation mobility within the cavity has been obtained [2] but not

studied. In addition the H_2 adsorption isotherms are usually recorded on dehydrated samples under cryogenic conditions, usually at 77 K, after the sample degassing by heating under moderate vacuum. All these factors: crystal water molecules removal, cation mobility and low temperature could be contributing to a probable reversible structural transition in that series of porous solids. Such a possibility was evaluated in this study from X-ray diffraction (XRD) powder patterns recorded for hydrated and anhydrous samples of $Zn_3A_2[Fe(CN)_6]_2 \cdot xH_2O$ with A=Na, K, Rb and Cs both at room temperature and at 77 K. As a reference material, $Zn_3[Co(CN)_6]_2$ was also studied. This last composition, in its rhombohedral modification, is iso-structural to the Zn–Fe series, and it is free of exchangeable metal and of water molecules within the cavities. The XRD data were complemented with IR spectra recorded for both hydrated and anhydrous samples. The samples to be studied were previously characterized from energy-dispersed spectroscopy (EDS), infrared (IR), Mössbauer and thermogravimetric (TG) data. No previous studies on the cation mobility and structural changes on the water molecules removal for this series of porous solids have been reported.

2. Experimental

The samples to be studied were prepared as already reported [9,10], in summary: hot aqueous solutions (0.01 M) of zinc chloride and $K_4[Fe(CN)_6] \cdot 3H_2O$ (or $K_3[Co(CN)_6]$) were mixed, and the resulting precipitate was separated after 2 days of aging

* Corresponding author. On leave from Institute of Materials Science and Technology, University of Havana, Cuba. Tel./fax: +52 55 53954147.
E-mail address: ereguera@yahoo.com (E. Reguera).

within the mother liquor at 60 °C. The obtained solid was washed several times with distilled water in order to remove all the accompanying ions and then dried in air until it had constant weight. For Zn ferrocyanide, the solid precipitate from sodium ferrocyanide was also prepared. The nature of the obtained solids as hexacyanometallates was confirmed from IR spectra. The metals atomic ratio in the studied samples was estimated from EDS analyses, using a spectrometer (from Noran Co.) coupled to a SEM microscope (from Jeol Co.). The hydration degree (number of water molecules per formula unit) and dehydration temperature were estimated from TG curves. Mixed compositions of Zn ferrocyanides with A=Rb and Cs were prepared through ionic exchange from $Zn_3Na_2[Fe(CN)_6]_2 \cdot xH_2O$ in hot aqueous solutions according to a reported procedure [7].

The XRD powder patterns were recorded with $\lambda=1.55019$ Å (7.99802 keV) using the LNLS synchrotron radiation facility (Campinas, Brazil), at room conditions before and after the samples dehydration by moderate heating under continuous evacuation, and then on cooling down to 77 K. Once the sample is dehydrated, it was returned to room temperature and XRD patterns recorded. The temperature of heating was taken as the temperature where the sample becomes anhydrous, according to the TG curve recorded under high resolution mode to minimize kinetic effects. The XRD data were plotted in Q units ($2\sin\theta/\lambda$). The obtained XRD patterns were indexed, the cell parameters calculated and the crystal structure was solved by the Patterson methods and then refined using the Rietveld method implemented in the FullProf algorithm [13] and pseudo-Voigt peak shape function. Peak profiles were calculated within 10 times the peak width at half maximum. The background was modeled by a third-order polynomial. Details on the refinement parameters are available from Supplementary materials. The interatomic C–N distance was constrained to take values within certain limits considering results from single crystal studies in analog compositions [5,6].

The anhydrous samples to be studied by IR spectroscopy are immersed in Nujol (mineral oil) once extracted from the furnace and the spectra recorded using the Nujol mulls technique in order to avoid their rehydration by interaction with humid air. For comparison, the spectra for the hydrated samples were collected by the same procedure.

3. Results and discussion

3.1. Characterization of the samples to be studied

The samples under study correspond to previously characterized materials [9,10] and herein only a summary of their features is provided. Additional information of their structural and spectroscopic characterization is available from Supplementary materials. This series of porous solids crystallizes with a rhombohedral unit cell in the R-3c space group where the zinc atom has tetrahedral coordination to N ends of CN groups. Related to this coordination mode for the Zn atom, the material has a porous framework formed by cavities of about $12.5 \times 9 \times 8$ Å^3 communicated by elliptical windows of ~ 5 Å [5–10]. The charge balancing metal (A$^+$) is found close to the cavity windows because the framework negative charge is concentrated on the N atoms. In hydrated samples the metal (A$^+$) has coordinated water molecules in its environment. The cavity filling is completed by additional water molecules stabilized through hydrogen bonding interactions with the coordinated ones. Fig. 1 shows the TG curves for the series of materials under study. As expected the temperature of heating required to remove both weakly bonded and coordinated water molecules depends on the polarizing power of the involved metal (A$^+$), and it results,
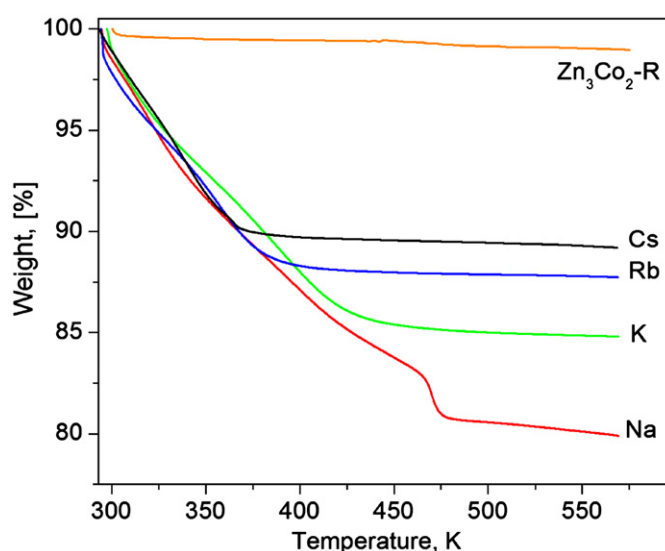

Fig. 1. TG curves for the series $Zn_3A_2[Fe(CN)_6]_2 \cdot xH_2O$ with A=Na, K, Rb and Cs and the reference compound $Zn_3[Co(CN)_6]_2$ (Zn$_3$Co$_2$-R).

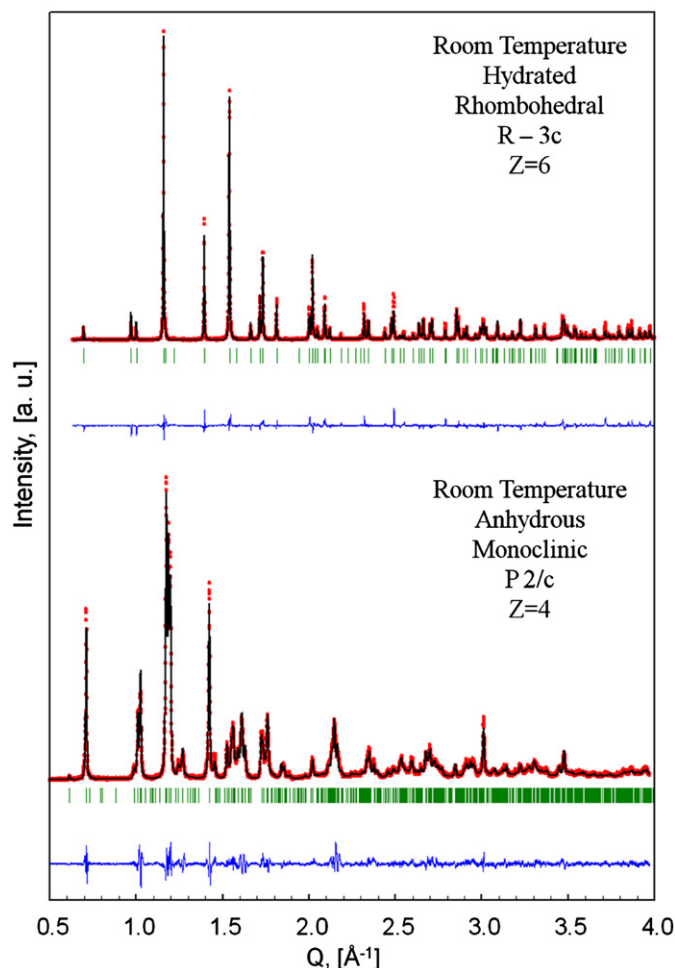**Fig. 2.** XRD powder patterns for $Zn_3K_2[Fe(CN)_6]_2$ in its hydrated (R-3c) and anhydrous (P2/c) phases. Analog XRD patterns were obtained for the remaining A metals.

in K: Na (473), K (436), Rb (390) and Cs (370). The distance between the water molecule dipole moment and charge center for Na$^+$ is the smallest one within the series; this results in

the strongest electrostatic interaction between them and, in consequence, for this metal the highest dehydration temperature is observed (Fig. 1). The inverse is valid for Cs^+, the biggest cation within the considered alkali ions. Once the material is dehydrated it remains stable up to above 600 K. The dehydration process is reversible, if the anhydrous samples are exposed to humid air; water molecules are adsorbed to restore the hydrated phases.

$Zn_3[Co(CN)_6]_2 \cdot xH_2O$ is a hydrated species when obtained or aged in humid air at room temperature, crystallizing in the cubic unit cell typical of Prussian blue analogs [2,9] but, on heating, from about 330 K it becomes anhydrous. The water molecules removal is accompanied by a structural transition to form the rhombohedral phase (R-3c) typical for the $Zn_3A_2[Fe(CN)_6]_2 \cdot xH_2O$ series. The cavities of the rhombohedral modification for $Zn_3[Co(CN)_6]_2$, in the following labeled as Zn_3Co_2-R, are free of exchangeable ion (A^+) and of water molecules.

In the considered series of solids the inner metal (Fe, Co) is always found in low spin electronic configuration because CN group at the C end behaves as a strong ligand. The charge donated to the metal through the σ interaction is partially compensated by a relatively strong π-back donation from the metal toward the ligand. The charge removed from the inner metal (Fe, Co) is partially located on the most electronegative N atom. This favors the concentration of negative charge on the cavity windows.

Table 1
Cell parameters for the materials under study in their hydrated and anhydrous phases.

Composition	Temperature (K)	Unit cell and Z	Cell parameters (Å)	Cell volume change (%)
$Zn_3Na_2Fe_2 \cdot 9H_2O$	300	R-3c; $Z=6$	$a=b=12.4233$ (5) $c=33.4326$ (4) $\gamma=120°$; $V/Z=745$ Å³	–
$Zn_3Na_2Fe_2$	300	P2/c; $Z=4$	$a=18.082(3)$ $b=12.496$ (3) $c=11.529$ (8) $\beta=91.25$ (2)°; $V/Z=651$ Å³	-12.6
$Zn_3Na_2Fe_2$	77	P2/c; $Z=4$	$a=18.097$ (8) $b=12.570$ (6) $c=11.124$ (3) $\beta=90.9$ (6)°; $V/Z=633$ Å³	-3.0
$Zn_3K_2Fe_2 \cdot 7H_2O$	300	R-3c; $Z=6$	$a=b=12.549$ (7) $c=32.2138$ (4) $\gamma=120°$; $V/Z=732$ Å³	–
$Zn_3K_2Fe_2$	300	P2/c; $Z=4$	$a=17.2610$ (9) $b=12.709$ (1) $c=12.266$ (7) $\beta=91.23$ (1)°; $V/Z=673$ Å³	-8.1
$Zn_3K_2Fe_2$	77	P2/c; $Z=4$	$a=17.151$ (3) $b=12.810$ (4) $c=12.187$ (1) $\beta=91.6$ (6)°; $V/Z=669$ Å³	-0.5
$Zn_3Rb_2Fe_2 \cdot 6H_2O$	300	R-3c; $Z=6$	$a=b=12.4956$ (9) $c=32.6394$ (8) $\gamma=120°$; $V/Z=736$ Å³	–
$Zn_3Rb_2Fe_2$	300	P2/c; $Z=4$	$a=17.765$ (8) $b=12.421$ (3) $c=12.9962$ (4) $\beta=93.19$ (7)°; $V/Z=716$ Å³	-2.7
$Zn_3Rb_2Fe_2$	77	P2/c; $Z=4$	$a=17.775$ (6) $b=12.449$ (5) $c=12.999$ (9) $\beta=93.7$ (1)°; $V/Z=718$ Å³	$\sim +$
$Zn_3Cs_2Fe_2 \cdot 5.6H_2O$	300	R-3c; $Z=6$	$a=b=12.4923$ (1) $c=32.8506$ (9) $\gamma=120°$; $V/Z=740$ Å³	–
$Zn_3Cs_2Fe_2$	300	P2/c; $Z=4$	$a=17.7654$ (1) $b=12.5394$ (7) $c=12.963$ (1) $\beta=91.88$ (5)°; $V/Z=722$ Å³	-2.5
$Zn_3Cs_2Fe_2$	77	P2/c; $Z=4$	$a=17.833$ (8) $b=12.510$ (7) $c=13.035$ (2) $\beta=92.5$ (1)°; $V/Z=727$ Å³	$\sim +$
Zn_3Co_2	300	R-3c; $Z=6$	12.4847 (3) 12.4847 (3) 32.756 (1) $\gamma=120°$; $V/Z=4421.5$ (2) Å³	–
Zn_3Co_2	77	R-3c; $Z=6$	12.486 (3) 12.486 (3) 32.766 (3) $\gamma=120°$; $V/Z=4423.8$ (6) Å³	$\sim +$

3.2. Structural changes on the water molecules removal

On the water molecules removal under moderate heating and continuous evacuation the recorded XRD powder pattern reveals the occurrence of a structural transition, from rhombohedral (R-3c) to monoclinic (P2/c) (Fig. 2). When the sample is rehydrated the rhombohedral structure is restored, indicating that the observed changes correspond to a reversible structural transition. In Table 1 the calculated unit cell parameters are summarized. The observed monoclinic distortion (β), up to 94°, suggests the occurrence of certain distortion also for the cavity shape, probably related to the cation position within the cavity (discussed below). In the hydrated phase the two (A^+) ions within a given cavity are found close to opposite windows in order to minimize the repulsive interaction between them and in a crossed configuration relative to their position in neighboring cavities. This leads to symmetrical cavities, of ellipsoidal shape. The water molecules removal is accompanied by cell volume contraction per formula unit, which depends on the involved exchangeable metal (A^+) and, in consequence, on the amount of water molecules found within the cavity. The maximum cell volume contraction, about 12%, is observed for Na^+, where the largest amount of water molecules within the cavity is found; for K^+ it is 8%, and for Rb^+ and Cs^+, a contraction ∼2.7% results (see Table 1 and Fig. 3). When the water molecules are removed the framework undergoes certain charge redistribution in order to reduce the free volume, which is detected as the observed cell volume reduction. Such charge redistribution is closely related to the cation polarizing power and its stronger interaction with the negative material framework for the anhydrous phase (discussed below).

When the anhydrous samples are cooled down to 77 K, a slight additional cell volume change per formula unit is observed, which is about −3% for Na, −0.5% for K and slightly positive for Rb and Cs (see Table 1). For Na and K, the most polarizing cation within the series, a lower thermal energy (kT) favors a stronger electrostatic interaction with the material framework and it is detected as an additional volume contraction. For Rb and Cs the dominant contribution is the well-known negative thermal expansion for metal hexacyanometallates [14–16]. For rhombohedral Zn_3Co_2 a slightly positive cell volume change on cooling was also observed (see Table 1).

3.3. Refined crystal structures and cation mobility

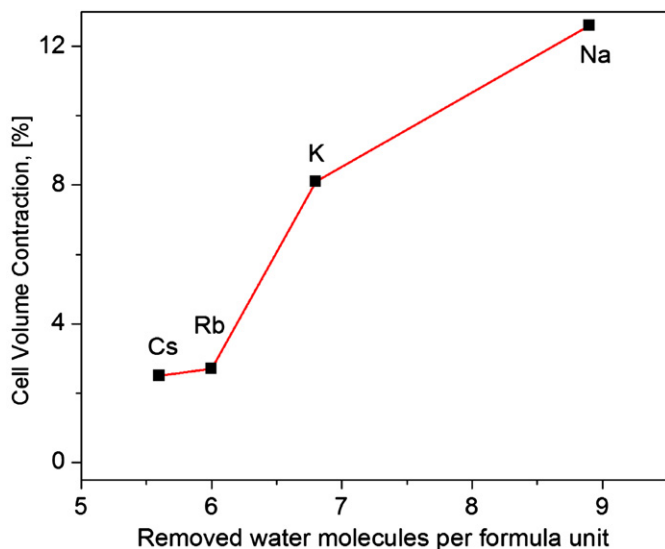The crystal structure was refined for A=K, Rb and Cs. For A=Na the recorded XRD powder pattern was of insufficient quality to be used for structural refinement. Fig. 4 shows the recorded, calculated and the difference profile from the Rietveld refinement of the anhydrous phases for these three exchangeable metals. The calculated atomic positions, interatomic distances, bond angles and thermal and occupation factors are available from Supplementary materials and were also deposited at the ICSD data base.

Compared to the hydrated phases the most pronounced changes on the water molecules removal are observed for the Zn–N interatomic distance and the N–Zn–N bond angle (Table 2). For the rhombohedral phase two slightly different Zn–N bond distances are observed, close to 1.98 Å, but for the monoclinic
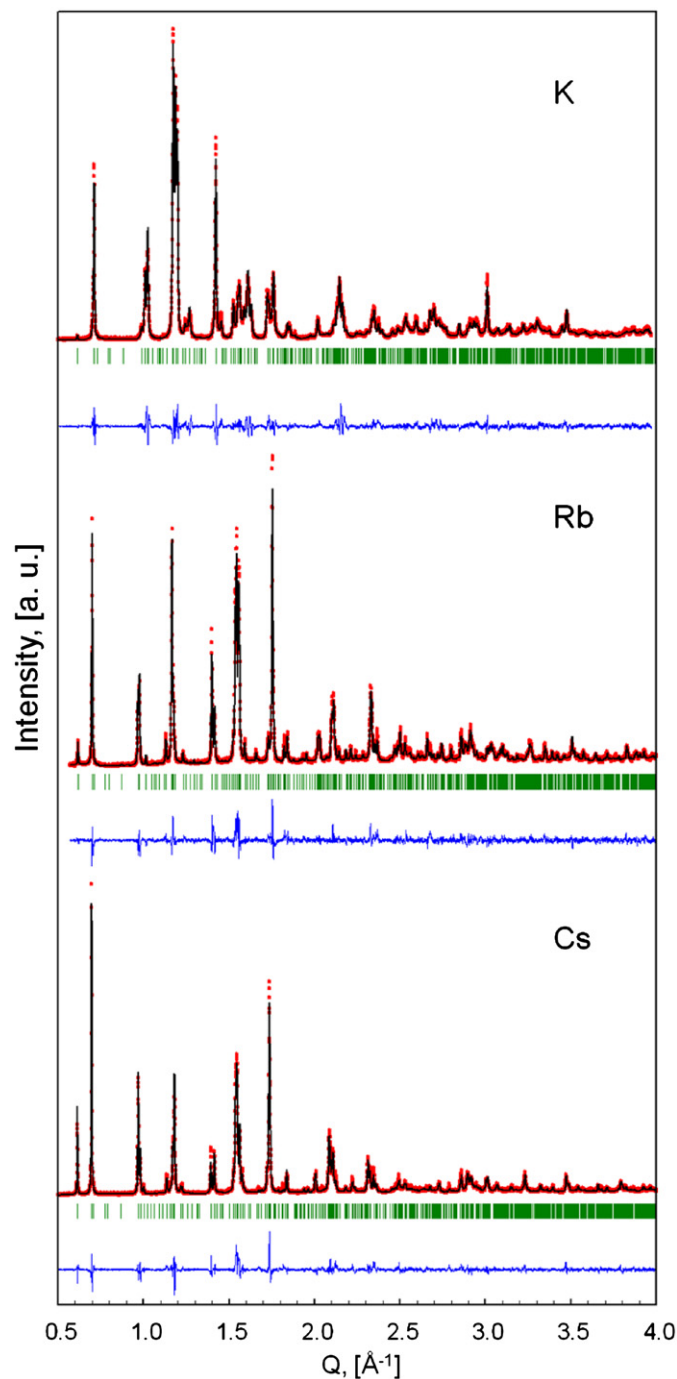

Fig. 3. Cell volume reduction on the water molecules removal.

Fig. 4. XRD powder patterns observed (red), calculated (black) and difference profile (blue) for the Rietveld refinement of the anhydrous phases of $Zn_3A_2[Fe(CN)_6]_2$ with A=K, Rb and Cs. (For interpretation of the references to color in this figure legend, the reader is referred to the web version of this article.)

Table 2
Relevant bond distances and angles for hydrated and anhydrous phases of $Zn_3A_2[Fe(CN)_6]_2 \cdot xH_2O$ with A=K, Rb and Cs.

Composition	Bond distance[a] (Å)	Bond angle[a] (deg.)	Cation–cation distance (Å)
$Zn_3K_2[Fe(CN)_6]_2 \cdot 7H_2O$	Fe–C=1.90 (4); Zn–N=1.97 (1)	Fe–C–N=176.7 (8); Zn–N–C=158.5 (9)	K–K=5.32 (1)
$Zn_3Rb_2[Fe(CN)_6]_2 \cdot 6H_2O$	Fe–C=1.91 (3); Zn–N=1.98 (2)	Fe–C–N=177.2 (1); Zn–N–C=156.9 (4)	Rb–Rb=6.07 (1)
$Zn_3Cs_2[Fe(CN)_6]_2 \cdot 5.6H_2O$	Fe–C=1.90 (3); Zn–N=1.97 (5)	Fe–C–N=173.6 (1); Zn–N–C=162.6 (2)	Cs–Cs=7.18 (1)
$Zn_3K_2[Fe(CN)_6]_2$	Fe–C=1.90 (1); Zn–N=2.00 (3)	Fe–C–N=162.9 (1); Zn–N–C=151.8 (1)	K–K=5.97 (1)
$Zn_3Rb_2[Fe(CN)_6]_2$	Fe–C=1.90 (7); Zn–N=2.02 (1)	Fe–C–N=167.6 (3); Zn–N9C=151.9 (2)	Rb–Rb=7.05 (1)
$Zn_3Cs_2[Fe(CN)_6]_2$	Fe–C=1.89 (5); Zn–N=2.04 (3)	Fe–C–N=166.9 (2); Zn–N–C=153.9 (3)	Cs–Cs=8.28 (1)

[a] Average bond distances and angles.
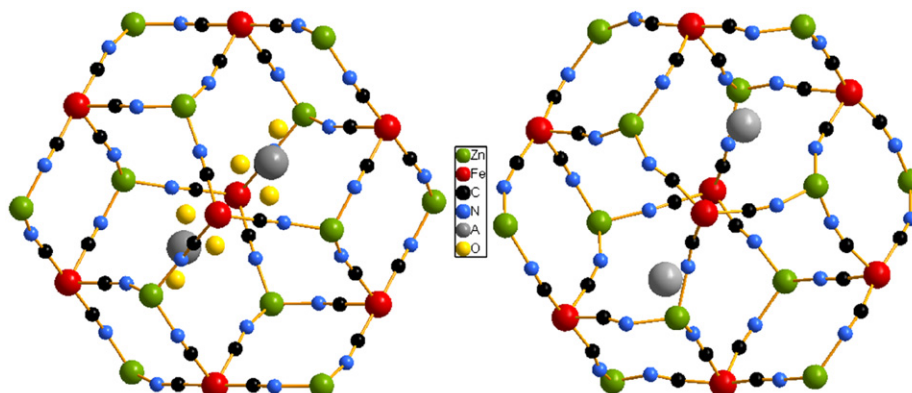
Fig. 5. Cation position in the hydrated (left) and anhydrous (right) forms of $Zn_3A_2[Fe(CN)_6]_2$. On the water molecules removal the cation migrates to favor a stronger electrostatic interaction with the framework negative charge, which is mainly located on the N ends of the CN bridges. The illustrated positions correspond to the most populated structural sites for the cation.

one, a relatively large variation for that distance was detected (see Supplementary materials), with an average value of 2.02 Å. The N–Zn–N bond angle changes from 159.3° in the hydrated phase to 152.5° for the anhydrous one. When the water molecules are removed the charge balancing cation (A^+) migrates in order to maximize the attractive metal–framework electrostatic interaction. This also minimizes the repulsive interaction between cations within a given cavity. The calculated increase for the metal–metal distance, from the refined crystal structures, is 0.65 Å(K^+), 0.98 Å(Rb^+) and 1.10 Å(Cs^+) (Table 2). In the anhydrous phase the cation is found near the N ends of the CN groups (Fig. 5). The cation migration toward the N ends induces changes in the framework electronic structure. A decrease in the distance between the cation and the N atom favors a stronger polarization for the negative charge on this last one, reducing the CN ligand ability to donate charge to the Zn atom. This is detected as the observed increase for the Zn–N interatomic distance, which is equivalent to a weakening for the Zn–N bond. In addition, when the cation approximates the N ends, at the coordination environment for the Zn atom, the repulsive electrostatic interaction between the two metal centers (A and Zn) is favored and this also contributes to the sensed weakening of the Zn–N bond. The observed monoclinic distortion on the water molecules removal and the detected variation for the Zn–N distance can be ascribed to the cation mobility. Since not all the available structural sites for the cation are equally populated slightly different Zn–N distances result (see Supplementary materials). This leads to certain structural distortion.

The recorded IR spectra for hydrated and anhydrous samples of $Zn_3A_2[Fe(CN)_6]_2 \cdot xH_2O$ (Fig. 6) support the above discussed evidence
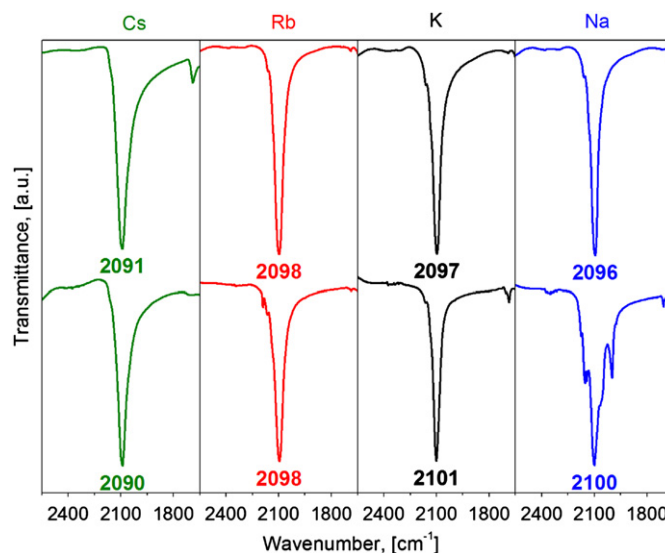
Fig. 6. IR spectra (ν(CN) region) for hydrated (above) and anhydrous (below) forms of $Zn_3A_2[Fe(CN)_6]_2 \cdot xH_2O$. The spectra were recorded in Nujol mulls in order to avoid the rehydration of the anhydrous phases.

on the cation–framework obtained from the structural study. The main IR sensor for metal hexacyanometallates is the frequency for the ν(CN) stretching vibration [17]. For Na^+ and K^+ a frequency increase of $4\,cm^{-1}$ was observed. These two metals are the most polarizing ones within the considered series. In cyanometallates the charge subtraction at the N end takes place through the 5σ orbital,

which has certain anti-bonding character, and from this fact, it is sensed as an increase for the frequency of the ν(CN) vibration. For Na^+ the frequency shift is accompanied by a notable splitting for the CN stretching mode. This corresponds to a pronounced decrease for the local symmetry around the N end, removing the degenerating character of this vibration. This band splitting also supports the above discussed structural transition, from rhombohedral to monoclinic, on the water removal. No appreciable frequency variation on the water removal was observed for Rb^+ and Cs^+, the bigger and less polarizing metals.

The above discussed structural transition on the samples dehydration for zinc zeolite-like hexacyanometallates (II) is relevant for their behavior as porous solids since the transition involves a change for the cavity shape and volume and also for the geometry of its windows. In the anhydrous phase the cation is found at the cavity windows and this probably hinders the diffusion of even small molecules. A cation is a charge center able to polarize the adsorbate electron cloud, reducing its diffusion rate. For instance, the reported kinetic effects for the hydrogen adsorption in $Zn_3Na_2[Fe(CN)_6]_2$ [2] can now be understood as resulting from a strong electrostatic interaction of the hydrogen molecule with the Na^+ atom located at the cavity windows. For $A=K^+$, Rb^+ and Cs^+, which are less polarizing cations, no kinetic effects are observed but evidence of their mobility is obtained.

4. Conclusions

When zinc zeolite-like hexacyanometallates (II) are dehydrated the charge balancing cation migrates to a position near N ends of the CN bridges, where the negative charge is concentrated, in order to maximize the strength for the cation–framework electrostatic interaction. The cations migration toward the cavity windows also minimizes the repulsive electrostatic interaction between them. This interaction favors the charge subtraction from the framework through a polarization mechanism, which was corroborated from the recorded IR spectra. This leads to a weakening of the Zn–N bond detected as a larger Zn–N distance and to a cavity distortion. The cation migration to a position near the windows explains the reported kinetic effects observed for the hydrogen adsorption in $Zn_3Na_2[Fe(CN)_6]_2$; Na^+ is a small cation that polarizes the electron cloud of the hydrogen molecule, reducing its diffusion rate. The results herein discussed are relevant for the potential applications of this family of porous solids in adsorption and separation processes. This study also suggests that in porous materials of molecular nature, which have a relatively soft framework, on the activation process and then when the samples are cooled for their characterization from adsorption data, the possibility of structural transitions occurrence cannot be ignored.

Supplementary information

Structural information derived from the crystal structures refinement for the anhydrous samples of the materials under study has been deposited at ICSD Fachinformationszentrum Karlsruhe (FIZ) (E-mail: CrysDATA@FIZ-Karlsruhe.DE) with ICSD file numbers: 421892: $Zn_3K_2[Fe(CN)_6]_2$; 421893: $Zn_3Rb_2[Fe(CN)_6]_2$; 421894: $Zn_3Cs_2[Fe(CN)_6]_2$.

Acknowledgement

Appendix A. Supplementary material

Supplementary material associated with this article can be found in the online version at doi:10.1016/j.jpcs.2011.05.012.

References

[1] S.S. Kaye, J.R. Long, Chem. Commun. (2007) 4486.
[2] L. Reguera, J. Balmaseda, L.F. del Castillo, E. Reguera, J. Phys. Chem. C 112 (2008) 5589.
[3] L. Reguera, C.P. Krap, J. Balmaseda, M. Ávila, E. Reguera, J. Phys. Chem. C 112 (2008) 17443.
[4] C. Rodríguez, E. Reguera, M. Ávila, J. Phys. Chem. C 114 (2010) 9322.
[5] P. Gravereau, E. Garnier, A. Hardy, Acta Crystallogr. B 35 (1979) 2843.
[6] P. Gravereau, E. Garnier, A. Hardy, Acta Crystallogr. B 38 (1982) 1401.
[7] E. Garnier, P. Gravereau, Rev. Chim. Miner. 20 (1983) 68.
[8] E. Garnier, P. Gravereau, K. Ahmadi, A. Hardy, Rev. Chim. Miner. 21 (1984) 144.
[9] J. Rodríguez-Hernández, E. Reguera, E. Lima, J. Balmaseda, R. Martínez-García, H. Yee-Madeira, J. Phys. Chem. Solids 68 (2007) 1630.
[10] M. Ávila, L. Reguera, C. Vargas, E. Reguera, J. Phys. Chem. Solids 70 (2009) 477.
[11] G. Turnes Palomino, M.R. Llop Carayol, C.Otero Areán, J. Mater. Chem. 16 (2006) 2884.
[12] F.J. Torres, B. Civalleri, A. Terentyev, P. Ugliengo, C. Pisani, J. Phys. Chem. C 111 (2007) 1871.
[13] J. Rodriguez-Carvajal, FullProf 2005 Program, Institute Louis Brillouin, Saclay, France, 2005.
[14] S. Margadonna, K. Prassides, A.N. Fitch, J. Am. Chem. Soc. 126 (2004) 15390.
[15] K.W. Chapman, P.J. Chupas, C.J. Kepert, J. Am. Chem. Soc. 128 (2006) 7009.
[16] A.L. Goodwin, M. Calleja, M.J. Conterio, M.T. Dove, J.S.O. Evans, D.A. Keen, L. Peters, M.G. Tucker, Science 319 (2008) 794.
[17] K. Nakamoto, in: Infrared Spectra of Inorganic and Coordination Compounds, John-Wiley & Sons, New York, Chichester, Brisbane, Toronto, Singapore 1995.